Radiation Physics and Chemistry 190 (2022) 109774

Contents lists available at ScienceDirect

Radiation Physics and Chemistry

journal homepage: www.elsevier.com/locate/radphyschem

Study of ^{99}Mo and long-lived impurities produced through (p, x) reactions in the ^{nat}Mo

Arshiya Anees Ahmed [a,*], Aleksandra Wrońska [a,**], Andrzej Magiera [a], Ryszard Misiak [b], Mirosław Bartyzel [b], Jerzy W. Mietelski [b], Bogdan Wąs [b]

[a] Marian Smoluchowski Institute of Physics, Jagiellonian University, Cracow, Poland
[b] H. Niewodniczański Institute of Nuclear Physics Polish Academy of Sciences, Cracow, Poland

ARTICLE INFO

Keywords:
^{99}Mo/^{99m}Tc
Proton induced reaction
Reaction cross section

ABSTRACT

Using the stack-foil activation technique, excitation functions were measured for (p, x) reactions on ^{nat}Mo target. The target was irradiated with a proton beam of 17 MeV kinetic energy. Along with the medically important radioisotopes ^{99}Mo/^{99m}Tc we studied other long-lived radio-impurities produced in the target. Cross sections of all the produced radioisotopes from ^{nat}Mo(p,x) reactions are compared with the available literature data, which show good agreement.

1. Introduction

In different fields of science and technology, carrier-free radioisotopes are used for many applications (Khandaker et al., 2007). Two major reactors that were used to produce medical radioisotopes faced sudden failures in the previous decade. Due to these, radioisotopes production methods based on charged particle accelerators were developed and are more favorable in many aspects (Scholten et al., 1999; Lagunas-Solar et al., 1991; National Research Council, 2009; Takács et al., 2003). Medium-energy particle accelerators are becoming a viable option for radioisotope production.

The importance of ^{99m}Tc in medicine is well known; about 80% of the nuclear medicine procedures utilise ^{99m}Tc radionuclide (Tárkányi et al., 2012). ^{99m}Tc decays to ^{99}Tc with a half-life of 6 h through 140.5 keV photon emission. Due to the small half-life, in many applications ^{99m}Tc is produced from its parent ^{99}Mo radioisotope ($t_{1/2}$ = 65.94 h). The majority of ^{99}Mo is produced through reactor-based fission reactions with enriched uranium-235, i.e. the ^{235}U(n,f)^{99}Mo reaction. However, many of the reactors that are involved in the production of medical radioisotopes are scheduled for shutdown within the next few years, due to their aging. Hence, over the longer run, the reactor-based production will become unreliable (Starovoitova et al., 2014).

The ^{99}Mo/^{99m}Tc can be produced using proton beams through the following reactions ^{100}Mo(p,pn)^{99}Mo and ^{100}Mo(p,$2n$)^{99m}Tc. The proton induced reactions on molybdenum were studied in detail by many research groups (Khandaker et al., 2006; Scholten et al., 1999; Lagunas-Solar et al., 1991; Takács et al., 2002, 2003, 2015; Tárkányi et al., 2012, 2019; Bonardi et al., 2002; Alharbi et al., 2011a, 2011b; Chodash et al., 2011; Lebeda and Pruszyński, 2010; Červenák and Lebeda, 2016; Qaim et al., 2014; Szkliniarz et al., 2017; Gagnon et al., 2011; Elbinawi et al., 2020), but the cross-section data show significant discrepancies (e.g. the discrepancy between the literature data is about a factor 2 in magnitude in the case of ^{99m}Tc around 10 MeV proton energy). Determination of the optimum irradiation conditions for the production requires precise cross-section data as input. Also, such data are of importance for other applications such as medical science, environmental science, accelerator technology, astrophysics, space, and aviation technology (Khandaker et al., 2007).

In this work, we present results of a direct measurement for the production cross section of ^{99}Mo, ^{99m}Tc and other long-lived radio-isotopes produced through (p, x) reactions on ^{nat}Mo by a standard stack-foil activation technique up to 17 MeV proton energy.

* Corresponding author.
** Corresponding author.
E-mail addresses: arshiya.anees.ahmed@doctoral.uj.edu.pl (A.A. Ahmed), aleksandra.wronska@uj.edu.pl (A. Wrońska).

https://doi.org/10.1016/j.radphyschem.2021.109774
Received 20 May 2021; Received in revised form 23 August 2021; Accepted 31 August 2021
Available online 15 September 2021

Table 1
Isotopic composition of ^{nat}Mo target taken from Ref (Meija et al., 2016).

Isotopes	Abundance (%)
^{92}Mo	14.64
^{94}Mo	9.18
^{95}Mo	15.87
^{96}Mo	16.67
^{97}Mo	9.58
^{98}Mo	24.29
^{100}Mo	9.74

Table 2
Nuclear data for radionuclides produced via proton-induced reactions in a ^{nat}Mo target (Nuclear data, 2020; NuDat 2.8; Chu et al., 1999). Gamma ray energies used in the analysis are in bold. Uncertainties of the half-life, photon energies and the corresponding intensities in the last valid digits are in italics.

Radio-Nuclide	$t_{1/2}$	E_γ [keV]	I_γ [%]	Contributing reactions	Q-value [MeV]
^{93}Tc	2.75 h *5*	**1363.02 *4***	**66**	^{92}Mo(p,γ)	4.086
		1477.13 *4*	8.7 *5*	^{94}Mo$(p,2n)$	−13.661
		1520.37 *9*	24.4 *8*	^{95}Mo$(p,3n)$	−21.030
				^{96}Mo$(p,4n)$	−30.185
				^{93m}Tc decay	
^{94}Tc	293 min *1*	**702.622 *19***	**99.6 *18***	^{94}Mo(p,n)	−5.038
		849.74 *7*	95.7 *18*	^{95}Mo$(p,2n)$	−12.407
		871.09 *18*	99.9	^{96}Mo$(p,3n)$	−21.562
		993.91 *18*	2.21 *3*	^{94m}Tc decay	
		1522.11 *20*	4.5 *3*		
		1868.68 *8*	5.7 *3*		
^{95}Tc	20.0 h *1*	**765.794 *7***	**93.82 *19***	^{94}Mo(p,γ)	4.896
		947.67 *2*	1.951 *19*	^{95}Mo(p,n)	−2.473
		1073.71 *2*	3.74 *4*	^{96}Mo$(p,2n)$	−11.627
				^{97}Mo$(p,3n)$	−18.448
				^{95m}Tc decay	
^{95m}Tc	61 d *2*	**204.117 *2***	**63.25 *13***	^{94}Mo(p,γ)	4.896
		582.082 *3*	29.96 *5*	^{95}Mo(p,n)	−2.473
		835.149 *5*	26.63 *19*	^{96}Mo$(p,2n)$	−11.627
				^{97}Mo$(p,3n)$	−18.448
^{96}Tc	4.28 d *7*	314.337 *71*	2.43 *19*	^{96}Mo(p,n)	−3.756
		778.224 *15*	**99.9**	^{97}Mo$(p,2n)$	−10.577
		812.581 *15*	**82 *4***	^{98}Mo$(p,3n)$	−19.219
		849.929 *13*	98 *4*	^{96m}Tc decay	
		1126.965 *21*	15.2 *12*		
^{99m}Tc	6.01 h *1*	**140.511 *1***	**89**	^{98}Mo(p,γ)	6.500
				^{100}Mo$(p,2n)$	−7.796
				^{99}Mo decay	
^{99}Mo	65.94 h *1*	140.55 *1*	89.43 *23*	^{100}Mo(p,pn)	−8.294
		181.063 *8*	**5.99 *7***		
		366.421 *15*	1.191 *13*		
		739.50 *2*	**12.13 *12***		

2. Materials and methods

2.1. Experimental procedure

The target setup consisted of six metallic discs of natural molybdenum of 25 mm diameter, 0.1 mm thickness and 99.9% purity sandwiched between copper foils of 0.01 mm thickness. Isotopic composition of the ^{nat}Mo target is given in Table 1. The copper foils were used for beam current monitoring.

An external beam line of the AIC-144 cyclotron in the Institute of Nuclear Physics Polish Academy of Sciences, Cracow, Poland was used for irradiation. The cyclotron is an isochronous type, capable of delivering a 60 MeV collimated proton beam with 65 nA beam intensity. Since the beam energy cannot be regulated, we used a 99% pure aluminium foil of 13.2 mm thickness as an energy degrader. The average energy downstream of the degrader was calculated through the Geant4 simulation software (GEANT-4, 2017), and was found to be 17.5 MeV with a 0.8 MeV spread. The stack of targets was irradiated for 5 h, the targets were left to cool down for 8 h after the end of bombardment (EOB). The dimensions of the proton beam were measured using a fluorescent sheet placed at the Al degrader position. The beam diameter was found to be 5 mm before the degrader, 20 mm behind it, and 24 mm behind the entire target stack. Thus, the entire beam profile was contained in the target lateral dimensions.

2.2. Measurements and data analysis

The activity measurements were performed using an HPGe detector (type-p, 10% relative efficiency, energy resolution 3.4 keV FWHM at the 1332.5 keV peak of ^{60}Co, built in the Institute of Nuclear Physics PAN – Cracow) coupled with an ORTEC Multichannel Analyzers 919E Ether-NIM, which was used to register energy spectra of the gamma quanta emitted from the irradiated targets. . The efficiency calibration of the detector system was done using the ^{241}Am, ^{133}Ba, ^{109}Cd, ^{60}Co, ^{137}Cs and ^{22}Na standard sources. For routine control of energy calibration, we used the ^{152}Eu source. The detector was calibrated for different sample-detector geometries and the activity measurements were done in one of the geometries used for calibration, thus no interpolation of efficiency function was required. In all measurements the dead time of the detector was monitored and kept below 6% to avoid pile-up effect. Table 2 shows the nuclear data of the identified radioisotopes together with the reactions potentially contributing to their production (Nuclear data, 2020; NuDat 2.8; Chu et al., 1999). The resolution of the detector is $\sigma_E = 2.7$ keV for the 1173 keV γ-line, efficiency of the detector was 5%. To identify the radioisotopes, we conducted a series of measurements at different times after irradiation for each target foil. The data analysis proceeded as explained in Ref. (Ahmed et al., 2020). In the first step, the registered spectra were normalised to the detector live measurement time. Then the gamma peaks were fitted with a sum of Gaussian peaks and linear background yielding the peak integral count $\dot{N}$. The activities at the time of measurement were calculated according to the formula

$$A_{i,j} = \frac{\dot{N}_{i,j}}{f_j \varepsilon_j \tau_j \left(1 - e^{-t_{\mathrm{meas},i}/\tau_j}\right)}, \tag{1}$$

where the index i represents the measurement number in the sequence of collected spectra at different time after irradiation, j enumerates identified peaks, f_j is the relative emission probability per decay of a parent nucleus, ε_j stands for energy-dependent detector efficiency, τ_j is the mean lifetime and $t_{meas,i}$ denotes the duration time of the i-th measurement.

Subsequently, an exponential function (Eqn. 2) was fitted to the time dependence of $A_{i,j}$ to find the activity at the end of bombardment (A_{EOB}) for each identified peak j.

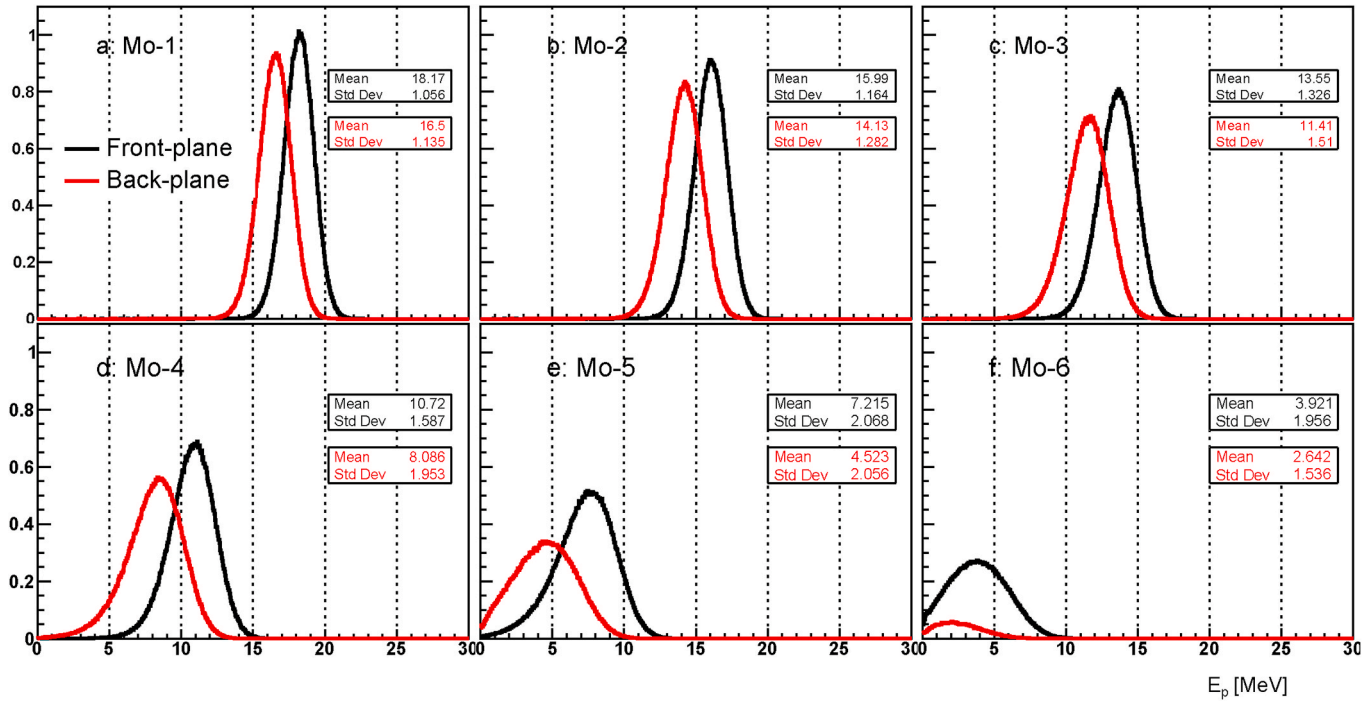

Fig. 1. Geant4-simulated energy distributions in the ^{nat}Mo targets, on the front surface (black) and back surface (red).

$$A_j(t) = A_{EOB,j}\exp(-t/\tau_j). \quad (2)$$

Plugging the A_{EOB} value into the standard activation formula we determined the reaction cross section σ [mb]

$$\sigma = \frac{ZeMA_{EOB}}{HN_A xI(1-e^{(-\lambda t_{irr})})}. \quad (3)$$

Here, Z is the atomic number of projectile, e is the elementary charge, M represents the atomic mass of the target material, H stands for the enrichment of the target, N_A is Avogadro's number, x is the target thickness, I is the beam current, λ denotes the decay constant of the radioisotope and t_{irr} represents the irradiation time.

2.3. Beam energy and current

To determine the energy degradation in the target stack, we performed Monte Carlo simulations using the Geant4 simulation software (GEANT-4, 2017). Fig. 1 shows the proton energy distribution in the subsequent ^{nat}Mo targets. The energy distribution in the targets is Gaussian for both proton beams entering and leaving the target. The energy range ΔE in the target is calculated as follows

$$\Delta E = E_{in} + \mathrm{HWHM}(E_{in}) - (E_{out} - \mathrm{HWHM}(E_{out})), \quad (4)$$

where E_{in} and E_{out} represent mean proton energies at the front and back plane of the target, respectively, and HWHM(x) stands for the half width at half maximum of the x variable distribution.

To verify the beam intensity experimentally, thin copper foils were used, as described in Sec. 2.1. Copper is an ideal material due to its physical, chemical and mechanical properties. Eqn. (3) was used to calculate the beam current. The nuclear reactions ^{nat}Cu$(p,x)^{62,63,65}$Zn are used to calculate the beam current based on the cross-section data of Ref. (Hermanne et al., 2018). The beam current value was deduced from each ^{nat}Cu target, the values were consistent for the whole set with a mean of 26 ± 1.5 nA.

Table 3
Experimentally determined cross sections of production of all the detected radioisotopes through the (p, x) reactions in a ^{nat}Mo target. Energy ranges in the targets as well as the point specific uncertainties of cross sections in the last valid digits are in brackets.

Proton energy [MeV]	Production cross section [mb] of different nuclei from the ^{nat}Mo(p,x) reactions						
	^{93}Tc	**^{94}Tc**	^{95}Tc	^{95m}Tc	^{96}Tc	^{99m}Tc	**^{99}Mo**
3.3(27)	0.82 (10)	0.92 (10)	3.47 (42)	2.54 (28)	1.45 (13)	1.38 (15)	1.01 (11)
5.9(38)	1.03 (12)	1.05 (11)	10.8 (12)	6.02 (66)	10.48 (95)	2.09 (22)	1.11 (12)
9.4(34)	1.71 (20)	7.31 (77)	55.7 (64)	28.8 (32)	104.8 (96)	49.8 (52)	2.16 (24)
12.5(27)	2.11 (25)	18.5 (20)	93 (11)	36.9 (41)	140 (13)	211 (22)	10.9 (12)
15.1(24)	13.6 (16)	51.8 (55)	116 (14)	50.1 (55)	125 (12)	242 (26)	34.9 (39)
17.3(21)	46.1 (53)	65.2 (69)	108 (13)	48.8 (54)	101.2 (91)	242 (26)	64.8 (72)

2.4. Estimation of uncertainties

The total uncertainty is divided into two parts: a *point specific uncertainty* and a *common absolute normalisation uncertainty*. The point specific one consists of the statistical uncertainty for the measured counts in the photo-peak, the uncertainty of the target foil thickness, and the uncertainty in nuclear decay data. The common uncertainty is composed of the accuracy of the detector efficiency and beam current determination. The point specific uncertainty ranges between 9 and 11%

3. Results and discussions

3.1. Cross sections of Tc isotopes production

The activation formula (Eqn. 3) was used to calculate the cross section. The obtained results, together with the corresponding

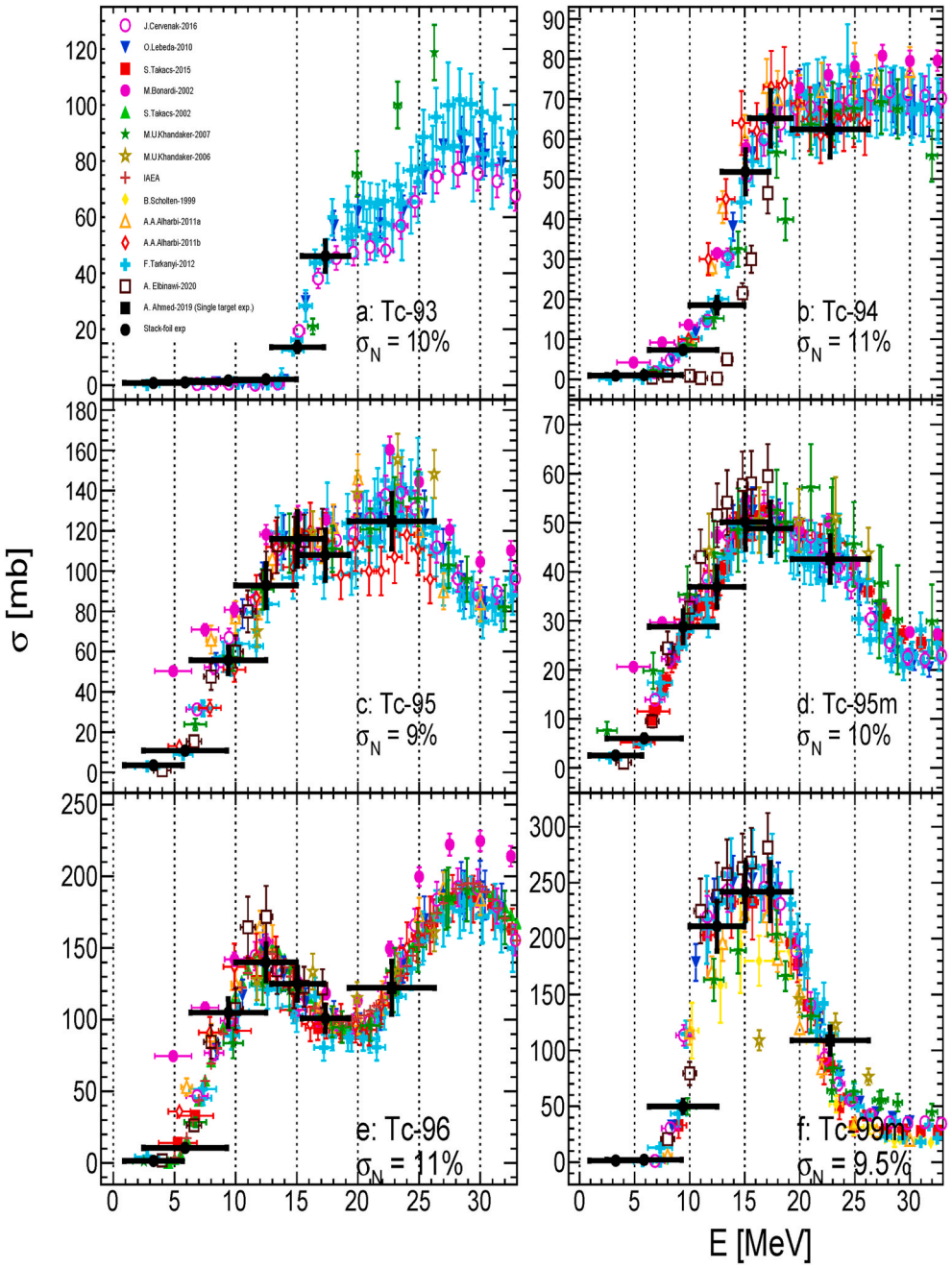

Fig. 2. Obtained production cross sections of $^{nat/100}$Mo(p,x) reactions (black circles) shown together with other existing data sets. The horizontal error bars represent the range of energy degradation within the ^{nat}Mo targets (eq. (4)), and the vertical ones the point specific cross-section uncertainty (see sec. 2.3). The uncertainty of absolute normalisation σ_N is stated in each panel.

uncertainties, are listed in Table 3. The literature data used for comparison were taken from EXFOR database (EXFOR database, 2020).

For the production of ^{93}Tc radioisotope, the dominant reaction in the investigated energy range is ^{94}Mo$(p,2n)$ and the decay of ^{93m}Tc ($t_{1/2}$ = 43.5 min), so the reported cross section is cumulative. Independent gamma line 1363 keV (66%) was used to determine the cross section of ^{93}Tc production. The contribution from the reaction ^{92}Mo(p,γ) dominates below 13.8 MeV. As shown in Fig. 2 (a) there is a good agreement between the present and the literature data (Khandaker et al., 2007; Tárkányi et al., 2012; Lebeda and Pruszyński, 2010; Červenák and Lebeda, 2016; Elbinawi et al., 2020). The data points of Ref (Khandaker et al., 2007). are considerably above the trend of other data sets for beam energies above 19 MeV.

To determine the formation cross section of ^{94}Tc, the photo-peak of 702.62 keV γ-line (99.6%) was used. We studied the excitation function of ^{nat}Mo $(p,x)^{94g}$Tc reaction only, and the contribution from ^{94m}Tc could be neglected due to the relatively short half-life of ^{94m}Tc compared to the measurement agenda, as discussed in Refs. (Lebeda and Pruszyński, 2010; Takács et al., 2015; Červenák and Lebeda, 2016; Qaim et al., 2014; Ahmed et al., 2019). From Fig. 2 (b), it is evident that the results obtained are in agreement with the literature data, except the data of Ref. (Khandaker et al., 2007), which are for higher beam energies.

The ^{95}Tc radioisotope has a long-lived isomeric state ^{95m}Tc($t_{1/2}$ = 61 days) and relatively short-lived ground state with $t_{1/2}$ = 20 h, electron capture process is the major decay mode. Th e ^{95}Tc activity measurement was based on the detection of 765.79 keV

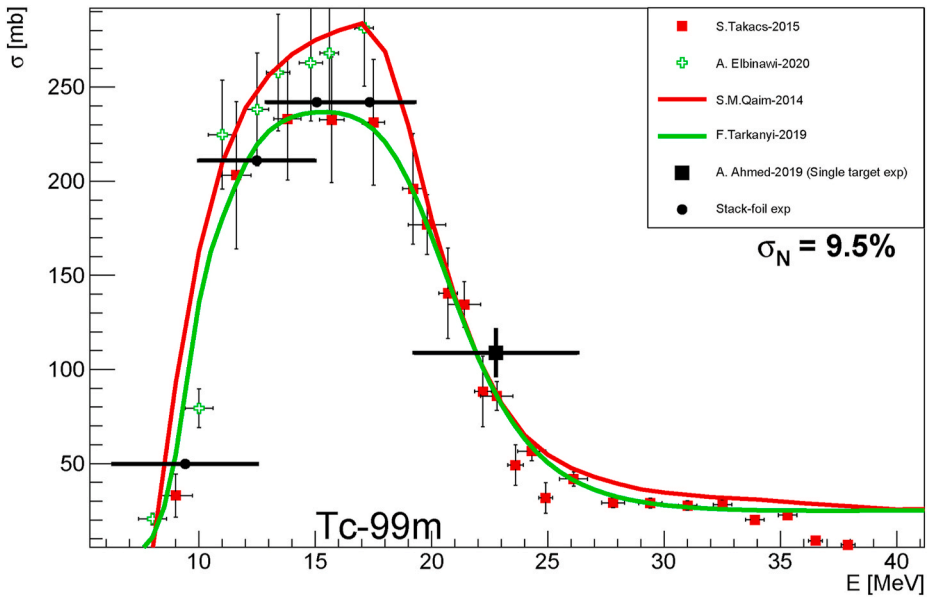

Fig. 3. Excitation function of ^{100}Mo(p, x)^{99m}TcTc reaction overlaid with the results of theoretical calculations of Refs (Tárkányi et al., 2019; Qaim et al., 2014). and very recent experimental data from Refs. (Takács et al., 2015; Elbinawi et al., 2020; Ahmed et al., 2019). The horizontal error bars represent the range of energy degradation within the ^{nat}Mo target (eq. (4)), and the vertical ones the point specific cross-section uncertainty (see sec. 2.3). The σ_N represents the uncertainty of absolute normalisation.

(93.82%) gamma line. Formation of ^{95}Tc is due to the ^{95}Mo(p,n) and ^{96}Mo$(p,2n)$ reactions with a small contribution from the ^{95m}Tc decay. The present data were compared with the available literature data and are shown in Fig. 2 (c); the present data are in good agreement with the literature data from Refs (Khandaker et al., 2006, Khandaker et al., 2007; Tárkányi et al., 2012; Bonardi et al., 2002; Alharbi et al., 2011a, 2011b; Lebeda and Pruszyński, 2010; Červenák and Lebeda, 2016; Elbinawi et al., 2020). within the uncertainties.

The long-lived ^{95m}Tc isomer is produced through the same processes as ^{95}Tc. Cross section calculations were done by considering 204.11 keV γ-line (63.25%). The interference of ^{95m}Nb (2.3%) photo-peak of the same energy was insignificant for the current proton energy range. The obtained radioisotope production cross section is consistent with the available literature data (Fig. 2 (d)).

The ^{96m}Tc ($t_{1/2}$ = 51.5 min) decays into ^{96}Tc through isomeric transition (98%) by emitting less intense gamma spectral lines that are not suitable for quantitative studies (Khandaker et al., 2006; Alharbi et al., 2011b). To measure the excitation function of ^{96}Tc we considered the photo-peaks 778.22 keV (99.9%) and 812.58 keV (82%) γ-lines. Because of short $t_{1/2}$ and the high isomeric transition decay rate of ^{96m}Tc, we can consider the measured cross section as the cumulative cross section of ^{96m}Tc and ^{96g}Tc. Fig. 2 (e) shows the comparison of the present data with the available database. Our data shows good agreement with all other reported data.

The ^{99m}Tc emits only 140.5 keV gamma quanta while decaying to the ground state, exploited in medical applications. The dominating route for the production of ^{99m}Tc radioisotope is via ^{100}Mo$(p,2n)^{99m}$Tc [natural abundance in ^{100}Mo is 9.74%], small contribution from

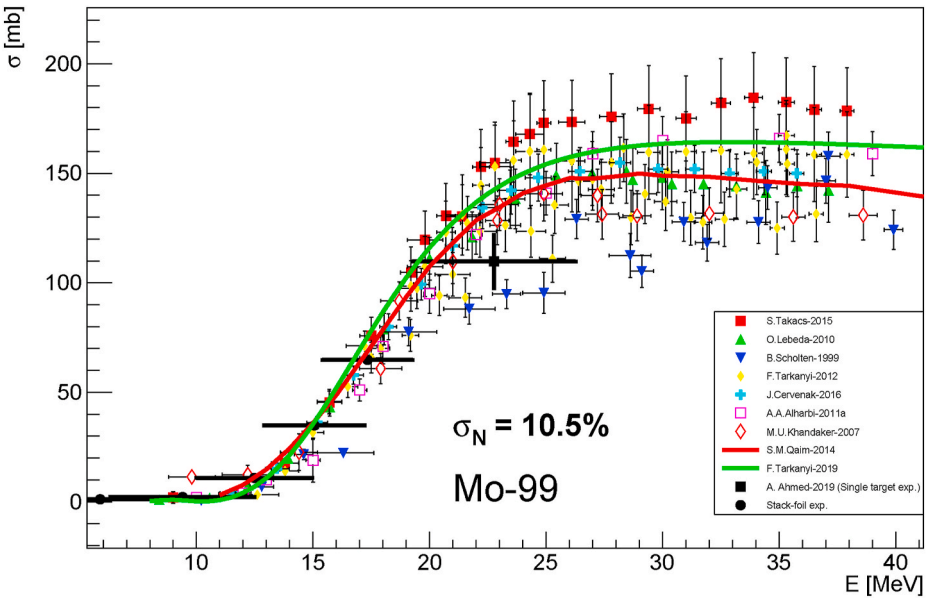

Fig. 4. Production cross section of ^{100}Mo$(p,x)^{99}$Mo reactions. The horizontal error bars represent the range of energy degradation within the ^{nat}Mo target (eq. (4)), and the vertical ones the point specific cross-section uncertainty (see sec. 2.3). The σ_N represents the uncertainty of absolute normalisation.

^{98}Mo$(p,\gamma)^{99m}$Tc reaction and the ^{99}Mo decay. Activity measurement of ^{99m}Tc was done by studying the 140.5 keV gamma line. The data analysis of this photopeak was done as discussed in Ref. (Ahmed et al., 2019). We have used ^{nat}Mo target, but the cross section of ^{99m}Tc presented here is after extrapolating to 97.4% of ^{100}Mo. Fig. 2 (f) shows the comparison of present and existing literature data. Good agreement is found with all data sets except the data of Refs. (Khandaker et al., 2006, Khandaker et al., 2007; Scholten et al., 1999), which have the same trend as others but lower cross-section values. A theoretical approach to model the production cross section of ^{99m}Tc and ^{99}Mo was presented in Ref (Qaim et al., 2014). and recently in Ref. (Tárkányi et al., 2019). In Fig. 3 the comparison of the present data with very recent literature data from Refs (Takács et al., 2015; Tárkányi et al., 2019; Qaim et al., 2014; Elbinawi et al., 2020; Ahmed et al., 2019). and the theoretical calculations are presented.

3.2. Cross section of ^{99}Mo production

The radioisotope ^{99}Mo emits very intense 140.55 keV [89.43%] radiation, but this gamma line interferes with the ^{99m}Tc line. Therefore, other transitions of smaller intensity were used: 181.06 keV [5.99%] and 739.5 keV [12.13%] to determine the ^{99}Mo production cross section. The production channels which contribute to the production of ^{99}Mo are: ^{100}Mo$(p,pn)^{99}$Mo and ^{100}Mo$(p,2p)^{99}$Nb, whereas ^{99}Nb ($t_{1/2}$ = 15 s) decays to ^{99}Mo through the β-decay. A comparison between our measured cross section, recalculated to the 97.4% abundance of ^{100}Mo in the target, and previously reported data is presented in Fig. 4. A satisfactory agreement is observed.

4. Summary and conclusions

The nuclear reactions ^{nat}Mo(p,x) were studied for proton beam energy range 2–17 MeV. We measured the cross section for the production of ^{93}Tc, ^{94}Tc, ^{95}Tc, ^{95m}Tc, ^{96}Tc, ^{99m}Tc and ^{99}Mo radioisotopes through the stacked foil technique on ^{nat}Mo using a proton beam. The determined cross sections have been compared with the available literature data and a good agreement within the uncertainties with most of the data sets was found. The present results add value to database and help to reduce the uncertainties as it was recommended by the authors of Ref. (Elbinawi et al., 2020), calling for more experimental results for proton induced reaction on Mo targets.

Authorship contributions

Conception and design of study: Arshiya Anees Ahmed, Aleksandra Wrońska, Andrzej Magiera.

Experiment and acquisition of data: Arshiya Anees Ahmed, Aleksandra Wrońska, Andrzej Magiera, Ryszard Misiak, Mirosław Bartyzel, Jerzy W. Mietelski, Bogdan Wąs.

Analysis and/or interpretation of data: Arshiya Anees Ahmed, Aleksandra Wrońska, Andrzej Magiera.

Drafting the manuscript: Arshiya Anees Ahmed, Aleksandra Wrońska;

Revising the manuscript critically for important intellectual content: Arshiya A. Ahmed, A. Wrońska, A. Magiera, R. Misiak.

Approval of the version of the manuscript to be published (the names of all authors must be listed): Arshiya A. Ahmed, A. Wrońska, A. Magiera, R. Misiak, M. Bartyzel, J. W. Mietelski, B. Wąs.

Declaration of competing interest

The authors declare that they have no known competing financial interests or personal relationships that could have appeared to influence the work reported in this paper.

Acknowledgment

This work was supported by the DSC-2017 and DSC-2019 grants intended to finance the development of young researchers and PhD students of Jagiellonian University at the Faculty of Physics, Astronomy and Applied Computer Science with the decision number MNiSW: 7150/E-338/M/2017 and N17/MNS/000003. The authors are grateful to the technical staff of Cyclotron Center Bronowice for the irradiation.

References

Ahmed, A.A., Wrońska, A., Magiera, A., Bartyzel, M., Mietelski, J.W., Misiak, R., Wąs, B., 2019. Reexamination of Proton-induced Reactions on ^{nat}Mo at 19–26 MeV and Study of Target Yield of Resultant Radionuclides. Acta Phys. Pol. B 50, 1583–1596.

Ahmed, A.A., Wrońska, A., Magiera, A., Curcio, A., Jaglarz, M., Wawrzyniak, A., 2020. Study of Mo99 and long-lived impurities produced in the ^{nat}Mo reactions using an electron beam. Radiat. Phys. Chem. 177, 109095.

Alharbi, A., Alzahrani, J., Azzam, A., 2011a. Activation cross-section measurements of some proton induced reactions on Ni, Co and Mo for proton activation analysis (PAA) purposes. Radiochim. Acta 99, 763–770.

Alharbi, A.A., Azzam, A., McCleskey, M., Roeder, B., Spiridon, A., Simmons, E., Goldberg, V., Banu, A., Trache, L., Tribble, R., 2011b. Medical radioisotopes production: a comprehensive cross-section study for the production of Mo and Tc radioisotopes via proton induced nuclear reactions on ^{nat}Mo. In: Singh, Nirmal (Ed.), Radioisotopes - Applications in Bio-Medical Science, pp. 3–26.

Bonardi, M., Birattari, C., Groppi, F., Sabbioni, E., 2002. Thin-target excitation functions, cross-sections and optimised thick-target yields for ^{nat}Mo$(p,xn)^{94g,95m,95g,96(m+g)}$ Tc nuclear reactions induced by protons from threshold up to 44 MeV. No Carrier Added radiochemical separation and quality control. Appl. Radiat. Isot. 57, 617–635.

Červenák, J., Lebeda, O., 2016. Experimental cross-sections for proton-induced nuclear reactions on ^{nat}Mo. Nucl. Instrum. Methods Phys. Res. Sect. B Beam Interact. Mater. Atoms 380, 32–49.

Chodash, P., Angell, C., Benitez, J., Norman, E., Pedretti, M., Shugart, H., Swanberg, E., Yee, R., 2011. Measurement of excitation functions for the ^{nat}Mo$(d,x)^{99}$Mo and ^{nat}Mo$(p,x)^{99}$Mo reactions. Appl. Radiat. Isot. 69, 1447–1452.

Chu, S.Y.F., Ekström, L.P., Firestone, R.B., 1999. Table of radioisotopes version 2.0, the Lund/LBNL nuclear data search. http://nucleardata.nuclear.lu.se/toi/index.asp.

Elbinawi, A., Al-abyad, M., Bashter, I., Seddik, U., Ditrói, F., 2020. Study of proton induced nuclear reactions on molybdenum: cross section measurements and theoretical calculations. Radiochim. Acta 108, 1–9.

EXFOR database, 2020. Experimental nuclear reaction data (EXFOR). Database version of August 29.2020. https://www-nds.iaea.org/exfor/exfor.htm.

Gagnon, K., Bénard, F., Kovacs, M., Ruth, T.J., Schaffer, P., Wilson, J.S., McQuarrie, S.A., 2011. Cyclotron production of ^{99m}Tc: experimental measurement of the ^{100}Mo$(p,x)^{99}$Mo, ^{99m}Tc and ^{99g}Tc excitation functions from 8 to 18 MeV. Nucl. Med. Biol. 38, 907–916.

GEANT-4, 2017. Geant4 (Simulation Software), vol. 2017, Version 10.2.3. http://geant4.web.cern.ch/geant4/index.shtml.

Hermanne, A., Ignatyuk, A., Capote, R., Carlson, B., Engle, J., Kellett, M., Kibédi, T., Kim, G., Kondev, F., Hussain, M., Lebeda, O., Luca, A., Nagai, Y., Naik, H., Nichols, A., Nortier, F., Suryanarayana, S., Takács, S., Tárkányi, F., Verpelli, M., 2018. Reference cross sections for charged-particle monitor reactions. Nucl. Data Sheets 148, 338–382.

Khandaker, M., Meaze, A.M.H., Kim, K., Son, D., Kim, G., Lee, Y., 2006. Measurements of proton-induced reaction cross-sections of ^{nat}Mo by using the MC50 cyclotron at the Korean institute of radiological and medical sciences. J. Kor. Phys. Soc. 48, 821–826.

Khandaker, M., Uddin, M., Kim, K., Lee, Y., Kim, G., 2007. Measurement of cross-sections for the (p,xn) reactions in natural molybdenum. Nucl. Instrum. Methods Phys. Res. Sect. B Beam Interact. Mater. Atoms 262, 171–181.

Lagunas-Solar, M.C., Kiefer, P.M., Carvacho, O.F., Lagunas, C.A., Cha, Y.P., 1991. Cyclotron production of NCA ^{99m}Tc and ^{99}Mo. An alternative non-reactor supply source of instant ^{99m}Tc and ^{99}Mo→^{99m}Tc generators. Int. J. Radiat. Appl. Instrum. 42, 643–657. Part A. Applied Radiation and Isotopes.

Lebeda, O., Pruszyński, M., 2010. New measurement of excitation functions for (p,x) reactions on ^{nat}Mo with special regard to the formation of ^{95m}Tc, ^{99}Tc, ^{99m}Tc and ^{99}Mo. Appl. Radiat. Isot. 68, 2355–2365.

Meija, J., Coplen, T.B., Berglund, M., Brand, W.A., Bièvre, P.D., Gröning, M., Holden, N. E., Irrgeher, J., Loss, R.D., Walczyk, T., Prohaska, T., 2016. Isotopic compositions of the elements 2013 (iupac technical report). Pure Appl. Chem. 88, 293–306.

National Research Council, 2009. Medical Isotope Production without Highly Enriched Uranium. The National Academies Press, Washington, DC.

Nuclear data, 2020. Nuclear Structure and Decay Data. https://www-nds.iaea.org/relnsd/vcharthtml/VChartHTML.html.

NuDat 2.8. National Nuclear Data Center, Brookhaven National Laboratory. https://www.nndc.bnl.gov/.

Qaim, S., Sudár, S., Scholten, B., Koning, A., Coenen, H., 2014. Evaluation of excitation functions of ^{100}Mo$(p,d+pn)^{99}$Mo and ^{100}Mo$(p,2n)^{99m}$Tc reactions: estimation of long-lived Tc-impurity and its implication on the specific activity of cyclotron-produced ^{99m}Tc. Appl. Radiat. Isot. 85, 101–113.

Scholten, B., Lambrecht, R., Cogneau, M., Ruiz, H., Qaim, S., 1999. Excitation function for the cyclotron production of ^{99m}Tc and ^{99}Mo. Appl. Radiat. Isot. 51, 69–80.

Starovoitova, V.N., Tchelidze, L., Wells, D.P., 2014. Production of medical radioisotopes with linear accelerators. Appl. Radiat. Isot. 85, 39–44.

Szkliniarz, K., Sitarz, M., Jastrzębski, J., J, J.C., Jakubowski, J., Kapinos, K., Kisieliński, M., Stolarz, A., Trzcińska, A., Wojtkowska, J., Zipper, W., 2017. Production efficiency and radioisotopic purity of ^{99m}Tc formed using the (p, 2n) reaction on highly enriched ^{100}Mo target. Mod. Phys. Lett. 32, 1740012–1 – 1740012–11.

Takács, S., Tárkányi, F., Sonck, M., Hermanne, A., 2002. Investigation of the ^{nat}Mo(p, x)^{96m}Tc nuclear reaction to monitor proton beams. In: New Measurements and Consequences on the Earlier Reported Data, Nuclear Instruments and Methods in Physics Research Section B: Beam Interactions with Materials and Atoms, 198, pp. 183–196.

Takács, S., Szücs, Z., Tárkányi, F., Hermanne, A., Sonck, M., 2003. Evaluation of proton induced reactions on ^{100}Mo: new cross sections for production of ^{99m}Tc and ^{99}Mo. J. Radioanal. Nucl. Chem. 257, 195–201.

Takács, S., Hermanne, A., Ditrói, F., Tárkányi, F., Aikawa, M., 2015. Reexamination of cross sections of the ^{100}Mo(p, 2n)^{99m}Tc reaction. Nucl. Instrum. Methods Phys. Res. Sect. B Beam Interact. Mater. Atoms 347, 26–38.

Tárkányi, F., Ditrói, F., Hermanne, A., Takács, S., Ignatyuk, A., 2012. Investigation of activation cross-sections of proton induced nuclear reactions on ^{nat}Mo up to 40 MeV: new data and evaluation. Nucl. Instrum. Methods Phys. Res. Sect. B Beam Interact. Mater. Atoms 280, 45–73.

Tárkányi, F., Ignatyuk, A.V., Hermanne, A., Capote, R., Carlson, B.V., Engle, J.W., Kellett, M.A., Kibedi, T., Kim, G.N., Kondev, F.G., Hussain, M., Lebeda, O., Luca, A., Nagai, Y., Naik, H., Nicols, A.L., Nortier, F.M., Suryanarayana, S.V., Takács, S., Verpelli, M., 2019. Recommended nuclear data for medical radioisotope production: diagnostic gamma emitters. J. Radioanal. Nucl. Chem. 319, 487–531.